

# The effect of canopy roughness density on the constitutive components of the dispersive stresses

Davide Poggi  Gabriel G. Katul

Received: 11 September 2007 / Accepted: 17 January 2008 / Published online: 13 February 2008  
Springer-Verlag 2008

**Abstract** How to represent the effects of variable canopy urban canopies. It was also shown that the spatial locations morphology on turbulence remains a fundamental challenge contributing most to the dispersive terms were in the length yet to be confronted. Planar averaging over some immediate vicinity downstream of the rods. In the deeper minimal area can be applied to average-out this sort of layers of sparse canopies, these positions contributed large spatial variability in the time-averaged mean momentum and negative stresses, but in the upper levels of the canopy, balance. Because of the multiply connected air-spaces they contributed large but positive stresses. Because the spatial averaging gives rise to covariance or dispersive longitudinal velocity spatial perturbation ( $\bar{w}''$ ) behind the stress terms that are produced by the spatial correlations of rods is negative, the switch in sign in these stresses was the time-averaged quantities. These terms are “unclosed” connected with the sign of the vertical velocity spatial and require parameterization, which to date remains lacking perturbation ( $\bar{w}''$ ). Simplified scaling arguments, using a simple scaling due to the absence of data. Here, some experiments reduced mean continuity equation and the vertical mean were conducted to quantify the magnitude and sign of the momentum balance for the flow field near the rods, offer dispersive stresses for a cylindrical canopy where the rod diameter as to why  $\bar{w}'' > 0$  in much of the lower canopy levels density was varied but the individual rod dimensions (rod diameter  $d_r$  about  $0.75h_c$ ) while  $\bar{w}'' < 0$  in the upper canopy levels. height  $h_c$  and rod diameter  $d_r$ ) remained the same. Quadrant analysis was used to explore the genesis of their spatial coherency inside the canopy for a wide range of rod densities. When compared to the conventional turbulent stresses, these dispersive stresses can be significant in the lowest layers of sparse canopies. For dense canopies, the dispersive terms remain negligible when compared to the conventional momentum fluxes at all the canopy levels, consistent with previous experiments in vegetated and urban canopies.

---

D. Poggi (✉)  
Dipartimento di Idraulica, Trasporti ed Infrastrutture Civili,  
Politecnico di Torino, Turin, Italy  
e-mail: davide.poggi@polito.it

G. G. Katul  
Nicholas School of the Environment and Earth Sciences,  
Duke University, Durham, NC, USA

G. G. Katul  
Department of Civil and Environmental Engineering,  
Duke University, Durham, NC, USA

**Introduction**  
One of the major challenges in canopy turbulence is how to represent the effects of the three dimensional and highly variable canopy morphology on particle dispersion, heat, mass, and momentum transfer, whether the canopy is urban or vegetated (Ruck and Adams 1991; Katul and Albertson 1999; Finnigan 2000; Hsieh et al. 2000; Macdonald 2000; Macdonald et al. 2000; Siqueira et al. 2000; Nathan et al. 2002; Soons et al. 2004; Belcher 2005; Katul et al. 2005; Nathan and Katul 2005; Cava et al. 2006; Juang et al. 2006). Theoretically, planar averaging of the main flow variables over some minimal area, often extending few canopy heights, must be employed. However, when planar averaging is applied to the time-averaged mean momentum balance, covariance terms arising from the spatial correlation of time-averaged quantities are produced (Raupach and Shaw 1982; Finnigan 2000; Nikora et al. 2001). These

spatial covariances are referred to as dispersive fluxes of Theory stresses and are among the least understood terms in the momentum equation for canopy flows. This is not surprising as these terms have traditionally evaded direct measurements until recently (see Table 1 for review).

Given this “knowledge gap”, the main objective is to present time experiments that quantify the magnitude and sign of the components of the dispersive stresses for where  $t$  is time,  $x_i$  ( $x_1 = x, x_2 = y, x_3 = z$ ) are the cylindrical canopy in which the rod density was varied from longitudinal, lateral, and vertical directions, respectively; sparse to dense but the rod dimensions remained the same. ( $u_1 = u, u_2 = v, u_3 = w$ ) are the instantaneous velocity components along  $i$ ;  $p$  is the pressure normalized by the mean fluid density;  $\nu$  is the kinematic viscosity;  $g$  is the gravitational acceleration, and  $\delta_{ij}$  is the Kronecker delta. When decomposing the flow variables into localized “hot-spots” that exhibit some coherency in temporal averages (denoted by overbar) and turbulent space, and in the quadrant plane formed by perturbations excursions from them (i.e.  $\phi_j = \bar{\phi}_j + \phi'_j$ ), and upon time-averaging the resultant equations, the conventional mean and vertical velocities. Such coherency can be exploited from momentum equation at a point is constructing a prognostic model for the dispersive stresses, though by no means the results here provide a “validity” to their over-all study.

$$\frac{\partial u_i}{\partial t} + \frac{\partial u_j u_i}{\partial x_j} = g \delta_{i3} - \frac{\partial p}{\partial x_i} + \nu \frac{\partial}{\partial x_j} \left( \frac{\partial u_i}{\partial x_j} \right) \quad \text{and} \quad \frac{\partial u_i}{\partial x_i} = 0$$

$$\frac{\partial \bar{u}_i}{\partial t} + \bar{u}_j \frac{\partial \bar{u}_i}{\partial x_j} = - \frac{\partial \bar{p}}{\partial x_i} + \frac{\partial \tau_{ij}}{\partial x_j}, \quad \text{where}$$

Table 1 A summary of the key findings about the importance of dispersive stresses from various experiments and simulations in vegetated and urban canopies

Study	Comments on dispersive fluxes
Wind tunnel and flume experiments	
(Raupach et al. 1986)	Wind tunnel experiments for dense canopies (rods). Dispersive fluxes are negligible
(Bohm et al. 2000)	Wind tunnel study with sparse vegetation. Dispersive fluxes for momentum can be significant in the lower canopy layers
(Cheng and Castro 2002)	Wind tunnel experiments for dense urban canopies (blocks). Dispersive fluxes are small and negligible when compared to the turbulent momentum fluxes
(Poggi et al. 2004)	Flume experiments with canopy (rods) density varying from sparse to dense. Dispersive fluxes can be large for sparse canopies, especially in the lower canopy layers, exceeding up to 30% of the momentum turbulent flux, but negligible for dense canopies. These conclusions were valid for two high Reynolds numbers
(Pokrajac et al. 2007)	Open channel flow near 2-dimensional rough beds (square roughness with uniform spacing resembling “k-type” flow—a type of flow in which the obstacles are at their densest arrangement to maximize the drag on individual roughness elements but minimize sheltering effects by minimizing wake interferences). Dispersive fluxes can be large near the interface
Field experiments	
(Katul et al. 1999)	A uniform pine plantation with leaf area index varying by 18%. The variation of fluxes for momentum and heat are small just above the canopy, but not for CO <sub>2</sub> and water vapor fluxes
(Christen and Vogt 2004)	Cork oak plantation with tree density of 76 trees ha <sup>-1</sup> and 8 measurement stations all positioned at $z/h = 0.18$ from the ground. Dispersive fluxes for momentum were about 15% of turbulent momentum flux, and for heat, they are 5% of the turbulent sensible heat flux
Simulations (LES or DNS)	
(Coceal et al. 2006)	Direct numerical simulations of turbulent flow over regular arrays of urban-like, cubical obstacles. Within the arrays, significant dispersive stresses were reported whereas immediately above the obstacles, the Reynolds stresses continue to dominate
(Martilli and Santiago 2007)	LES simulations over an array of cubes. Dispersive fluxes are similar in magnitude to turbulent fluxes inside the obstacles

$$\tau_{ij} = -\overline{u'_i u'_j} + \nu \left( \frac{\partial \overline{u}_i}{\partial x_j} + \frac{\partial \overline{u}_j}{\partial x_i} \right).$$

Because resolving every single canopy element and formulating it as a boundary condition to these equations is a daunting task in all practical problems, averaging these equations over some minimal control area becomes necessary. For a cylindrical canopy composed of equally spaced rods, this planar averaging area may be comparable to the distance between rods. Hence, for this case, variables are further decomposed into planar averages (denoted by angular brackets) with spatial excursions now defined from these planar averaged quantities. Using the standard convention (Raupach and Shaw 1982),  $\overline{\phi_j} = \langle \overline{\phi_j} \rangle + \overline{\phi''_j}$ , the spatially and temporally averaged momentum equation for non-stratified flows becomes

$$\frac{\partial \langle \overline{u}_i \rangle}{\partial t} + \langle \overline{u}_j \rangle \frac{\partial \langle \overline{u}_i \rangle}{\partial x_j} = -\frac{\partial \langle \overline{p} \rangle}{\partial x_i} + \frac{\partial \tau_{ij}^T}{\partial x_j} + H_{sf} F_c$$

where  $H_{sf}$  is known as the Heaviside step function which takes on the value of unity if the averaging plane intersects the rods, and zero otherwise. The emerging stresses now are given as

$$\tau_{ij}^T = -\langle \overline{u'_i u'_j} \rangle - \langle \overline{u''_i u''_j} \rangle + \nu \left( \frac{\partial \langle \overline{u}_i \rangle}{\partial x_j} + \frac{\partial \langle \overline{u}_j \rangle}{\partial x_i} \right)$$

and

$$F_c = -\left\langle \frac{\partial \overline{p''}}{\partial x_i} \right\rangle + \left\langle \nu \frac{\partial^2 \overline{u''_i}}{\partial x_j \partial x_j} \right\rangle.$$

All double primed terms arise because horizontal averaging and differentiation do not commute because of the multiply-connected air spaces within the canopy volume (Raupach and Shaw 1982). The stress tensor  $\tau_{ij}^T$  now contains the conventional Reynolds and viscous stresses and the newly formed dispersive stress terms  $\langle \overline{u''_i u''_j} \rangle$  resulting from the spatial correlations of the time-averaged velocity components within the averaging volume. Analogous to the conventional Reynolds stresses  $\langle \overline{u''_i u''_j} \rangle$  is not a priori known and must be empirically modeled via a closure scheme.

### 3 Experiments

The experiment was conducted at the hydraulics Laboratory, DITIC Politecnico di Torino, in a re-circulating rectangular flume (18 m long, 0.90 m wide  $b_w$ , and 1 m deep) with sidewalls made of glass to permit optical access. The water depth  $h_w$ , was maintained constant with an average value of 0.6 m for a re-circulating flow rate excess of 130,000, which ensures fully-developed turbulent  $Q_r \sim 120 \text{ l s}^{-1}$ . Note that, because the flume bottom is horizontal, the flow depth is gradually varied and the flow

is driven by the hydraulic grade line. Moreover, due to the low aspect ratio (ow width/ow depth was less than 2), secondary currents in the flume maybe relatively strong. In designing the experimental set-up, we were confronted with a two-faced dilemma. The ratio of the flow width to the flow depth had to be very large but, at the same time, the flow depth had to be sufficiently large to resolve adequately the flow field inside the canopy sub-layer. Hence, we had to select between two less than optimal solutions and decided on a low aspect ratio because we were more interested in exploring the canopy flow field. Nevertheless, preliminary measurements showed that, both close to the bottom and in the middle of the channel, the primary source of drag is the canopy resistance. This finding is perhaps due to the fact that the canopy is tall enough to deduce secondary currents.

The model canopy was composed of an array of steel cylinders, 4 mm in diameter ( $d_r$ ) and 12 cm in height ( $=h_c$ ). These cylinders were arranged in a regular pattern along the 9 m long test section. Velocity runs were collected for five canopy densities: 67, 134, 268, 536, and 1072 rods  $\text{m}^{-2}$ . These canopy densities can be used to estimate the element area density (i.e. frontal area per unit volume) using  $a = nd_r$ , and results in  $a = 0.27, 0.53, 1.07, 2.13,$  and  $4.27 \text{ m}^{-2}$ , respectively (hereafter D1, D2, D3, D4 and D5 from the sparsest to the densest). Note here that the porosity for the densest canopy is given by  $n_p = 1 - (\pi/4) a d_r = 0.99$ , which is sufficiently large to neglect any finite porosity effects on the flow. Also, the densest frontal area density resulted in a drag coefficient ( $C_d$ ) comparable to estimates reported for dense forested ecosystems with leaf area index ranging from 3.5 to 6.0 (Katul and Albertson 1998; Katul and Chang 1999; Katul et al. 2004). How well does this experimental set-up represents the flow statistics within dense vegetated canopies has been explored, for several flow and topography conditions, by our research group [see for example Poggi et al. (2004c; 2007); Poggi and Katul (2007)]. It is clear from these works that the vertical inhomogeneity in the main flow statistics within the modeled canopy compare well with the ensemble portrayal of CSL field experiments.

Multiple runs were used to measure the velocity by a two-component Laser Doppler Anemometer (LDA) employed in forward scattering mode. Here, a run consists of sampling  $u$  and  $w$  time series at a single location (between or above the rods) as shown in Fig. The sampling duration and frequency per run were 300 s and 2,500–3,000 Hz, respectively. Using the area-averaged (or bulk) velocity ( $U_b = Q_r (b_w h_w)^{-1} = 0.22 \text{ m s}^{-1}$ ), the bulk Reynolds number  $Re_b (=U_b h_w / \nu)$  was in excess of 130,000, which ensures fully-developed turbulent flows. The bulk Froude number was kept sufficiently low ( $Fr_r = U_b / \sqrt{g h_w} \ll 1$ ) ensuring no super-critical states

arise. The friction velocity ( $u_*$ ) for each of the five densities were determined from the maximum of the velocity profile, resulting in  $u_* = 0.014, 0.018, 0.023, 0.029, 0.039 \text{ m s}^{-1}$  for the sparsest to the densest canopy, respectively. Note that the flow conditions are certainly gradually varied so the flow is driven by the hydraulic measurement location (that is the same across all five rod grade line and not by the slope. The mean slope of the hydraulic grade line for each of these densities are 4, 11, 18,  $32 \times 10^{-5}$  from D1 to D5. Do to the fact that the flow is not uniform the velocity varies longitudinally. Nevertheless this variation is very small and can be neglected in the momentum budget.

The  $\bar{u}''$  and  $\bar{w}''$  were determined at 11 planar measurement locations per level as shown in Fig. These 11 locations were unevenly spaced between the rods and they were chosen such that sampling was densest within regions between the rods, where the flow statistics exhibited the largest spatial variability. At each of these 11 planar

positions, 15 runs in the vertical were sampled every 1 cm and analyzed for the five rod densities. The dispersive stresses at each vertical plane were computed as follows:

Let  $\alpha_i$  be the area-weight assigned to each of the 11 measurement location (that is the same across all five rod densities) as shown in Fig. The spatially-averaged flow statistics and dispersive stresses can be computed as

$$\langle \bar{u}'w' \rangle = \sum_{i=1}^{11} \alpha_i \bar{u}'w'_i, \langle \bar{u} \rangle = \sum_{i=1}^{11} \alpha_i \bar{u}_i, \langle \bar{w} \rangle = \sum_{i=1}^{11} \alpha_i \bar{w}_i$$

$$\bar{u}''_i = \bar{u}_i - \langle \bar{u}_i \rangle, \bar{w}''_i = \bar{w}_i - \langle \bar{w}_i \rangle, \langle \bar{u}'' \bar{w}'' \rangle = \sum_{i=1}^{11} \alpha_i \bar{u}''_i \bar{w}''_i$$

where,  $\alpha_1 = \alpha_2 = \dots \alpha_4 = 0.021$ ;  $\alpha_5 = \alpha_6 = \dots \alpha_{10} = 0.056$ ;  $\alpha_{11} = 0.583$ ,  $\sum_{i=1}^{11} \alpha_i = 1$ . Additional details about the flow setup, the velocity measurements, and the LDA operation (especially near the ground and the rods) can be found elsewhere (Poggi et al. 2003 2004a b, c).

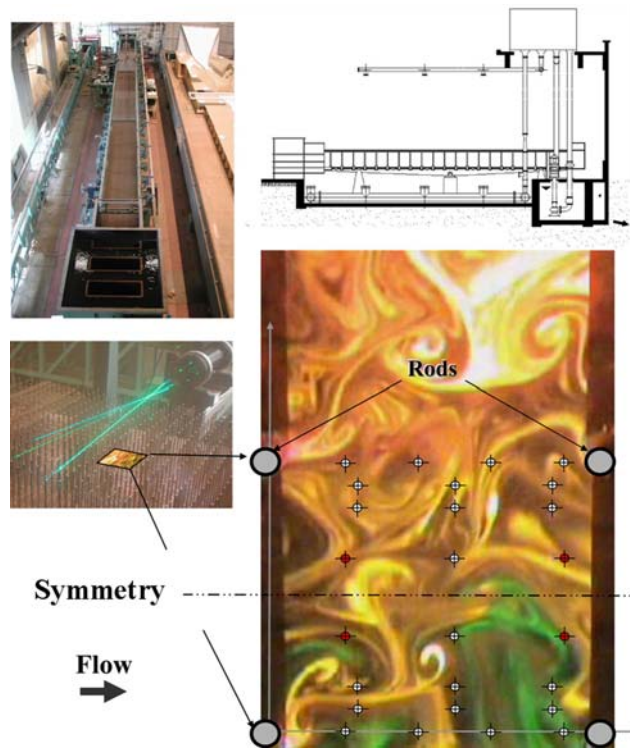


Fig. 1 Experimental setup displaying the recirculating flow and its cross-sectional schematic (a), the dense rod canopy and the LDA (bottom left), and the 11 sampling points (ten white dots) per level (bottom right) between the rods used in the dispersive flux calculations. When interpolating time-averaged quantities in space, lateral symmetry were employed. The red dots were symmetrically added to synthetically populate the “center” value with the only measurement in this region thereby adding robustness to the spatial interpolation scheme. A spatial snapshot of the dye relative concentration obtained from the laser-induced fluorescence (LIF) technique is also presented showing the formation of von Karman streets originating from the rods. Note the planar symmetry in the von Karman streets vortices

### 4 Results

Figure 2 shows the vertical variation of the computed  $\langle \bar{u}'' \bar{w}'' \rangle / u_*^2$  for all five rod densities along with the profiles of the conventional Reynolds stress  $\langle \bar{u}'w' \rangle / u_*^2$ , and the relative importance of the dispersive stresses with respect to the conventional Reynolds stress  $\langle \bar{u}'' \bar{w}'' \rangle / \langle \bar{u}'w' \rangle$ . Despite similarity in (a) rod lengths and diameters across the 5 rod density, and (b) sampling locations with respect to the rod positions, Fig 2 demonstrates that rod density does regulate the relative importance of the dispersive stresses when compared to the conventional turbulent stresses. In dense canopies, the dispersive stresses were found to be negligible when compared to the conventional momentum fluxes throughout (and when compared to the dispersive stresses in sparse canopies as well). Figure 3 presents the maximum recorded  $|\langle \bar{u}'' \bar{w}'' \rangle / \langle \bar{u}'w' \rangle|$  as a function of rod density showing that this maximum decreased significantly (by more than a factor of 10) with increasing rod density (by a factor of 15) suggestive that the isolated rod geometry alone cannot explain the magnitude (or sign as evidenced from Fig. 2) of the maximum dispersive stresses. The maximum  $|\langle \bar{u}'' \bar{w}'' \rangle / \langle \bar{u}'w' \rangle|$  occurred in the lower layers for the sparser canopies, and conversely, the maximum  $|\langle \bar{u}'' \bar{w}'' \rangle / \langle \bar{u}'w' \rangle|$  occurred in the upper 25% of the canopy for the densest case (and appears opposite in sign). These findings about the sign and magnitude are in agreement with Bohm et al. (2000) sparse canopy wind tunnel measurements, the dense urban canopy measurements reported by Cheng and Castro (2002), and the rod canopy wind tunnel experiments of

Fig. 2 Vertical variation of the dispersive stresses and the conventional Reynolds stresses for the five rod densities ( $\rho$ ). Rod density is increasing from D5 to D1

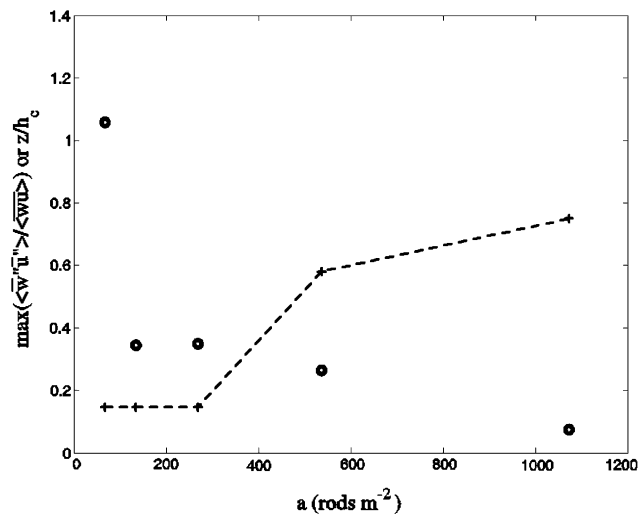
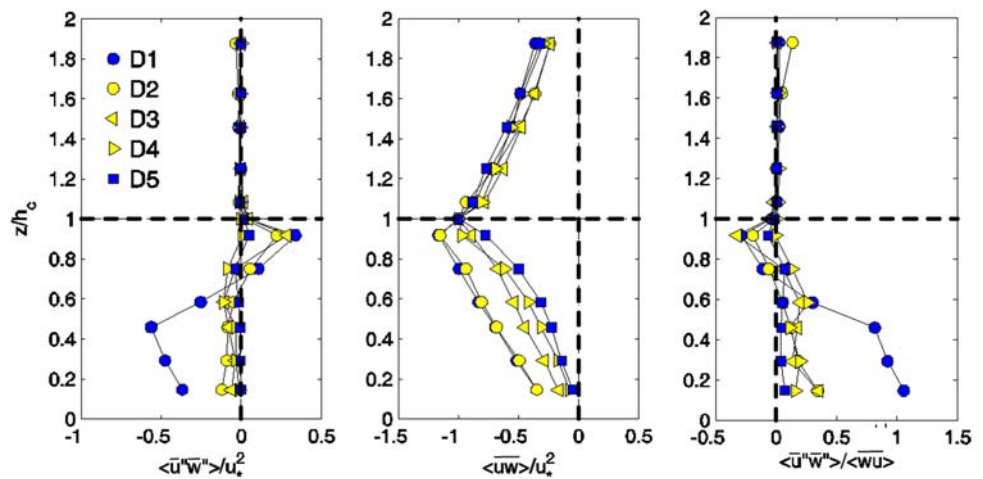
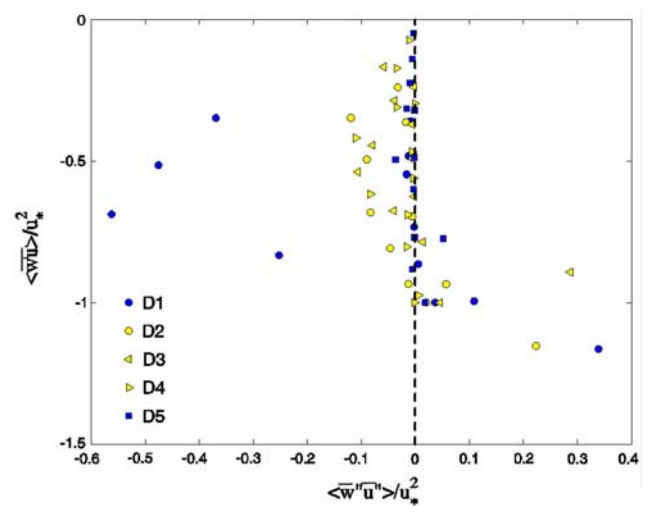


Fig. 3 The maximum dispersive stress inside the canopy as function of the rod density. The dotted line indicates the normalized height ( $z/h_c$ ) at which the maximum dispersive stresses occurred. Note that for small rod densities, these dispersive stresses occur near the ground, and conversely for large rod densities

Raupach et al. (1986). Figure 2 also suggests that the vertical structure of the dispersive stresses inside the canopy are not as tightly coupled to the vertical structure of the conventional Reynolds stresses, explicitly presented in Fig. 4 for clarity. Unlike the monotonic variations in  $\langle \bar{u}'\bar{w}' \rangle / u_*^2$  with  $z$  inside the canopy, the  $\langle \bar{u}''\bar{w}'' \rangle / u_*^2$  changes sign, from positive near the ground, to negative near the canopy top (Fig. 2). This sign shift, when taken together with the magnitude and elevation at which the maximum  $\langle \bar{u}''\bar{w}'' \rangle$ , (2)  $\bar{u}''$  is negative at these ‘hot-spots’ because of  $|\langle \bar{u}''\bar{w}'' \rangle| / \langle \bar{u}'\bar{w}' \rangle$  occurs, hints that dispersive stresses may be governed by a different mechanisms in the deeper canopy layers when compared to the upper canopy layers. To explore these mechanisms, the constitutive terms ( $\bar{u}''\bar{w}''$ ) at each of the 11 locations, sample heights, and rod densities are presented next.

Fig. 4 Comparison between the normalized dispersive stresses and conventional Reynolds stresses at all heights and rod densities

Figure 5a, b, and c show the planar variation of  $\bar{u}''\bar{w}''$ ,  $\bar{u}'\bar{w}'$ , and  $\bar{u}''\bar{w}'' / \bar{u}'\bar{w}'$  in the lower third, middle layers, and near the canopy top for the sparsest, intermediate, and densest canopies. These figures were produced from the 11 measurements collected at each  $z/h_c$  as shown in Fig. 1. An inverse-square distance scheme was used to interpolate between the 11 measurement points, and lateral symmetry was assumed. Not surprisingly, Fig. 5a–c suggest that (1) localized ‘hotspots’ situated immediately downstream from the rods are disproportionately contributing to the slow-down effects from the rods, and (2)  $\bar{u}''$  switches signs from positive near the ground to negative near the canopy top at these hotspots at around  $z/h_c = 0.75$  (derived from the more expansive data set discussed later; only a subset was shown in Fig. 2 for clarity). These spatial patterns appear qualitatively independent of the rod density



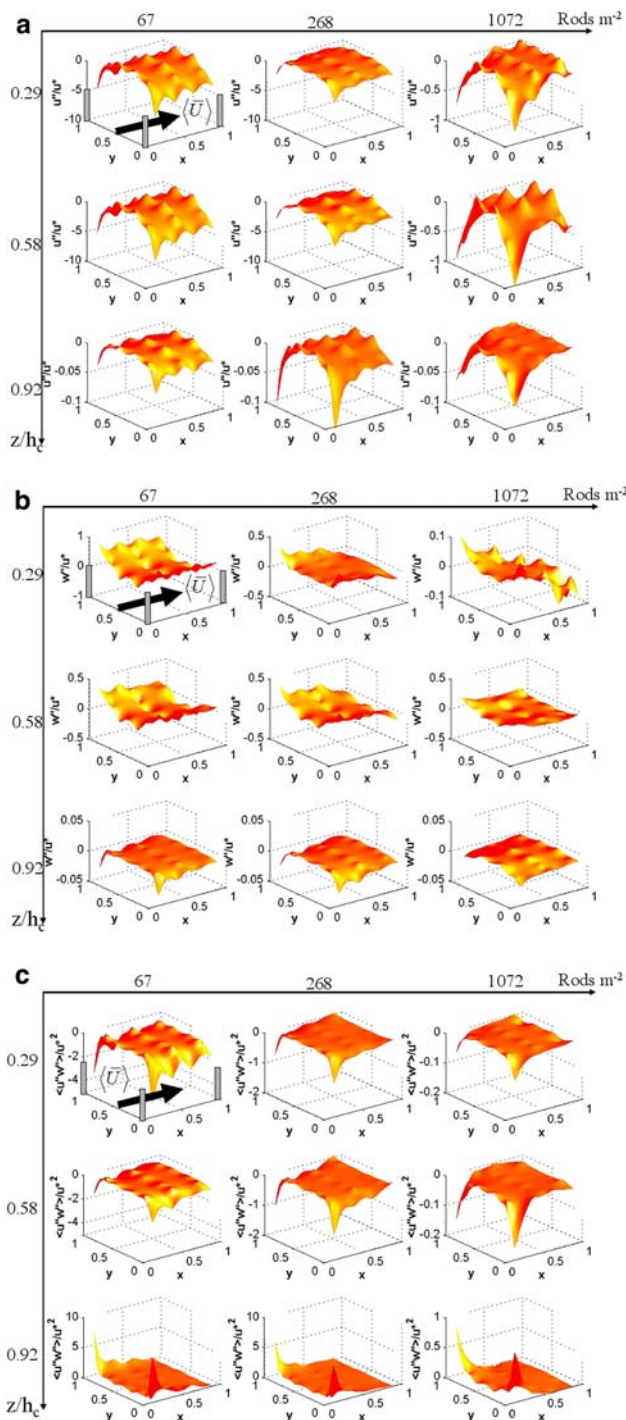


Fig. 5 a The spatial variation of the local  $\langle \bar{u}'' \rangle / u_*$  for three sample heights and for three rod densities (D1, D3 and D5). Adjacent to the rods,  $\bar{u}''$  is always negative as expected. Note the scale differences across the color plots: and  $y$  are the normalized distances between two adjacent rods (respectively in the longitudinal and lateral direction). b Similar to a but for  $\langle \bar{w}'' \rangle / u_*$ . Adjacent to the rods  $\bar{w}''$  appears positive in the bottom to middle layers but negative near the canopy top suggestive of two regimes impacting the dispersive terms. c Similar to a but for  $\langle \bar{u}'' \bar{w}'' \rangle / u_*^2$ . Note the sign shift near the rods for increasing  $z/h_c$  consistent with a, b

as shown in Fig 5a, b, but the relative contributions of these hotspots to  $\langle \bar{u}'' \bar{w}'' \rangle$  do vary appreciably with rod density as shown in Fig 5c.

The spatial coherency of the dispersive stresses is examined next via quadrant analysis. This analysis is conducted by plotting  $\langle \bar{w}'' \rangle / u_*$  versus  $\langle \bar{u}'' \rangle / u_*$  using all 11 planar locations (Fig 1) and the ve rod densities. The interpretation of the quadrant planes follows similar convention to the standard Reynolds stress except time excursions are now replaced by spatial perturbations. It is evident from Fig. 6 that for  $z/h_c < 0.75$ , all the large spatial perturbations reside primarily in quadrant four (i.e.  $\bar{w}'' > 0, \bar{u}'' < 0$ ) and the overall correlation between  $\langle \bar{u}'' \rangle / u_*$  and  $\langle \bar{w}'' \rangle / u_*$  appears strong and negative. For  $z/h_c > 0.75$ , the large perturbations mainly reside in quadrant 3 (i.e.  $\bar{w}'' < 0, \bar{u}'' < 0$ ) as expected from Fig 5a and b but their correlation is much weaker suggestive that other mechanisms is at play. At the hot spots, rods tend to slow down the uid immediately in their downstream vicinity when compared to the planar averages ( $\bar{u}'' < 0$ ) at the same height, yet  $\bar{w}'' > 0$  in the lower canopy layers and  $\bar{w}'' < 0$  in the upper canopy layers.

### 5 Discussion

From Figs. 5 and 6, the positive  $\bar{w}''$  in the hotspots of the lower canopy layers and the negative  $\bar{w}''$  in the hotspots of upper canopy layers clearly dictate the sign of the dispersive stresses. One possible explanation for this sign shift is illustrated in Fig. 7, which shows that just above the rods, the local mean continuity imposes a negative velocity if the flow is laterally homogeneous (hereafter referred to as the reduced continuity equation). However, near the ground, a positive vertical velocity adjacent to the rods may be anticipated because of the negative pressure gradients introduced by the rods. Possible scaling arguments for the sign shift in  $\bar{w}''$  are explored next.

#### 5.1 The negative vertical velocity near the canopy top

Above the canopy, we assume the flow to be almost homogeneous in the lateral direction so that  $\partial \bar{u} / \partial y \approx 0$ .

With this approximation, the reduced mean continuity equation just above the rod is

$$\frac{\partial \bar{u}}{\partial x} + \frac{\partial \bar{w}}{\partial z} = 0,$$

and results in  $\partial \bar{w} / \partial z = -\partial \bar{u} / \partial x < 0$ . The positive  $\partial \bar{u} / \partial x$  is due to the fact that at a given  $x$  just above the rods  $\bar{u}$  immediately after the rod is smaller than downstream

Fig. 6 Quadrant analysis for all points and all rod densities showing the events dominating the dispersive terms for  $z/h_c < 0.75$  and  $z/h_c > 0.75$ . These large excursions are situated in the hotspots nearest to the backface of the rods

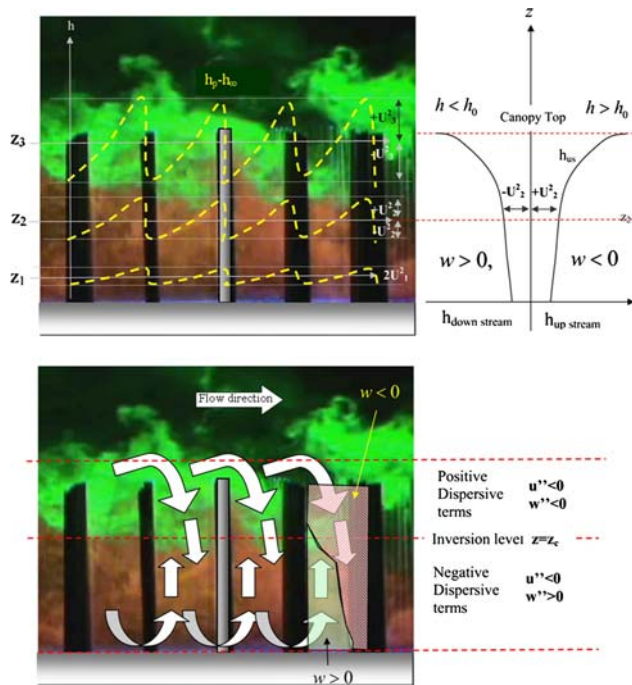
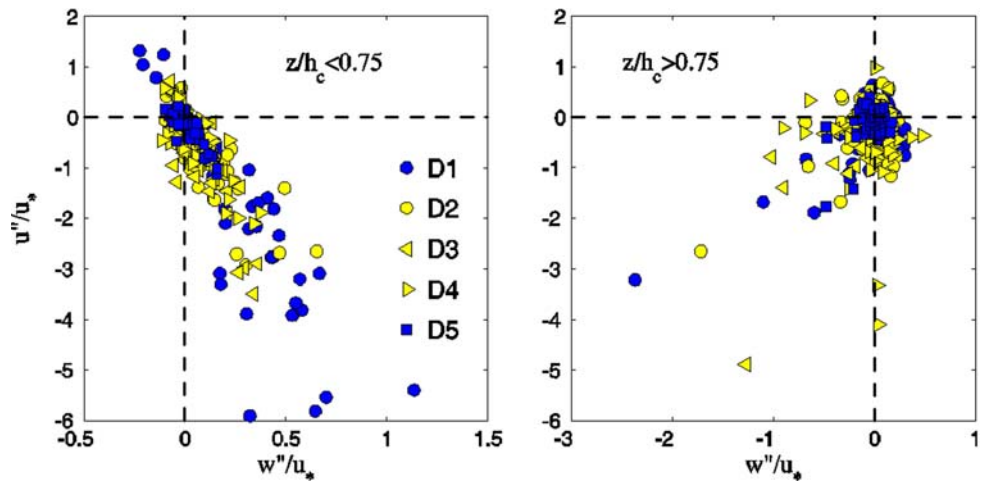


Fig. 7 Top left a schematic representation of the static head variations at three levels ( $z_1, z_2, z_3$ ) as a function of longitudinal distance between the centerlines of rods. For visual identification of the lower and upper canopy levels only, red dye was released from the ground and green dye was released from the canopy top. Top right schematic representation of as a function of for just upstream and just downstream from the rod. Bottom schematic representation of the expected flow based on the reduced continuity equation (upper canopy level) and static head variations (bottom canopy levels). Arrows indicate the direction of vertical movement between the centerlines of the rods. The origin of positive and negative dispersive stresses is also shown. In the figure  $U^2 = 1/2g \bar{u}_\infty^2$

the lowest layers of the canopy because the flow becomes three-dimensional and both  $\partial \bar{v} / \partial y \neq 0$ . We consider next possible mechanisms for the positive vertical velocity in these lower canopy layers.

### 5.2 The positive vertical velocity in the lower canopy layers

Recall from Figs 5 and 6 that a positive  $\bar{v}$  near the ground was measured in the hotspots, which cannot be predicted from the reduced mean continuity equation. This positive  $\bar{v}$  is not unique to the experiments here but has already been observed in other canopy flows at those layers (Nepf and Koch 1999). At the rod, pressure variations are large and are known to dominate vertical movement. These pressure variations are also known to be spatially inhomogeneous and, immediately next to the rod (to within several  $\bar{u}_\infty$ ), are often parameterised via the so-called pressure coefficient ( $=C_p$ ) given by (Nepf and Koch 1999)

$$C_p = \frac{h_p - h_{p_\infty}}{\frac{1}{2g} \bar{u}_\infty^2 - \frac{1}{2g} (\bar{u}^2 + \bar{v}^2)}$$

where  $h_p = p/(\rho g) + z$  is the hydraulic head at or near the rod,  $h_{p_\infty}$  and  $\bar{u}_\infty$  are the hydraulic head and velocity very far from the rod,  $\bar{u}$  and  $\bar{v}$  are the velocity components near the rod, assumed negligible relative to  $\bar{u}_\infty$ . This expression can be re-arranged to yield:

$$h_p \approx h_{p_\infty} + \frac{1}{2g} C_p \bar{u}_\infty^2$$

Immediately upstream from the rod  $C_p = 1$  due to stagnation from the rod (because the top of the rod imposes a no-slip condition). Assuming that  $\bar{v}$  at the top of the rod is also zero, the reduced mean continuity equation predicts that  $\bar{w} < 0$  immediately downstream from the rods (e.g. at the hotspot). However, this simplified analysis does not hold at (Achenbach 1968; Nepf and Koch 1999). When  $C_p = 1$ ,

Bernoulli’s equation for inviscid flows along a planar streamline from the rod is recovered. Immediately behind the rods, viscous effects and flow separation prohibit the usage of inviscid approximations.

Assuming that  $\bar{w} \propto -\partial h_p / \partial z \approx -C_p \bar{u}_\infty d \bar{u}_\infty / dz$  (i.e. assuming  $\partial h_{p\infty} / \partial z = 0$ , because  $p_\infty$  varies hydrostatically), and noting that  $d \bar{u}_\infty / dz > 0$  inside canopies, we find that  $C_p$  primarily controls the sign of  $\bar{w}$ . As earlier noted, in front of a cylinder,  $C_p$  is positive and  $\bar{w} < 0$ ; immediately behind the cylinder  $C_p$  is negative  $\bar{w} > 0$ , as illustrated in Fig. 7.

### 5.3 A unifying scaling argument

To “bridge” the arguments in Sects. 5.1 and 5.2, consider the local mean vertical momentum balance,

$$\bar{u} \frac{\partial \bar{w}}{\partial x} + \bar{w} \frac{\partial \bar{w}}{\partial z} + \bar{v} \frac{\partial \bar{w}}{\partial y} = -\frac{\partial}{\partial z} (h_p + \overline{w'w'}) - \dots = -\frac{\partial}{\partial z} (\Gamma),$$

where  $\Gamma$  includes the hydraulic head, turbulent stresses, and viscous terms. Let  $L_x$ ,  $L_y$ , and  $L_z$  represent the longitudinal, lateral, and vertical length scales over which gradients are to be approximated. The mean vertical momentum and mean continuity equations become

$$\begin{aligned} \bar{w} \frac{\delta \bar{w}}{L_z} &= -\frac{\delta \Gamma}{L_z} - \bar{u} \frac{\delta \bar{w}}{L_x} - \bar{v} \frac{\delta \bar{w}}{L_y}; & \delta \bar{w} &= -\delta \bar{u} \frac{L_z}{L_x} - \delta \bar{v} \frac{L_z}{L_y} \\ \Rightarrow \bar{w} &= -\frac{\delta \Gamma}{\delta \bar{w}} - \bar{u} \frac{L_z}{L_x} - \bar{v} \frac{L_z}{L_y} = -\left( \frac{\delta \Gamma}{\delta \bar{w}} \frac{\delta \bar{u}}{\delta \bar{w}} + \bar{u} \frac{L_z}{L_x} \right) \\ &- \left( \frac{\delta \Gamma}{\delta \bar{w}} \frac{\delta \bar{v}}{\delta \bar{w}} + \bar{v} \frac{L_z}{L_y} \right), \end{aligned}$$

where  $\delta$  represents flow variable differences.

To estimate  $\delta \Gamma / \delta \bar{u}$  and  $\delta \Gamma / \delta \bar{v}$  at the hotspot requires accounting for the numerous turbulent and viscous processes in addition to the hydraulic head. However, order of magnitude estimates of  $\delta \Gamma / \delta \bar{u}$  or  $\delta \Gamma / \delta \bar{v}$  may be derived by considering the region immediately connected to the cylinders as in Sect. 5.2. As before,  $\delta \Gamma / \delta \bar{u}$  and  $\delta \Gamma / \delta \bar{v}$  depends on  $C_p$  via

$$\frac{\delta \Gamma}{\delta \bar{u}} \approx -C_p \bar{u}; \quad \frac{\delta \Gamma}{\delta \bar{v}} \approx -C_p \bar{v}.$$

Setting  $C_p = -1$  results in

$$\bar{w} \sim \bar{u} \left( \frac{L_x}{L_z} - \frac{L_z}{L_x} \right) + \bar{v} \left( \frac{L_y}{L_z} - \frac{L_z}{L_y} \right).$$

Since we have no direct measurements of  $\bar{w}$ , we confine our analysis to  $\bar{u} \left( \frac{L_x}{L_z} - \frac{L_z}{L_x} \right)$  assuming that  $\left( \frac{L_x}{L_z} - \frac{L_z}{L_x} \right)$  dictates the sign of  $\bar{w}$ . This assumption may be reasonable if the impact of the turbulent wakes on the hotspots are governed by von Kármán streets (Poggi et al. 2004; Poggi

and Katul 2006), where their planar symmetry (as shown in Fig. 1) leads to  $L_y \sim L_x$ . The outcome of these simplifications is that the anisotropy in length scales  $(L_z - L_x / L_x)$  now governs the sign of  $\bar{w}$ . Also, the genesis of this anisotropy is now clearly linked to the two competing effects earlier described in Sects. 5.1 and 5.2. The first is a negative downward tendency produced by the reduced mean continuity equation and leads to  $\bar{w} L_z / L_x$ , and the second is a positive upward contribution resulting from the pressure forcing and the negative  $C_p$  behind the rods resulting in  $-C_p \bar{u} L_x / L_z$ .

Typical  $L_x$  may be formulated as some multiplier of the rod diameter (i.e.  $L_x = \lambda d_r$ ), where  $\lambda \geq 5$  to ensure that spatial gradients sample at least one von Kármán street vortex. Typical  $L_z$  may be commensurate with the canonical mixing length given as  $L_z = \alpha' (k z) + (1 - \alpha') (\beta h_c)$ , where  $\alpha' \in [0, 1]$  is determined by  $L_c / h_c$ ,  $L_c = (C_d \alpha)^{-1}$  is the adjustment length scale,  $C_d$  is the drag coefficient,  $\beta = k(1 - d_o / h_c)$ , and  $d_o$  is the zero-plane displacement height. For large  $d_o / h_c$  (i.e. very sparse canopies),  $\alpha' \rightarrow 1$  and boundary layer mixing lengths dominate  $L_z$ , and for small  $L_c / h_c$  (i.e. dense canopies),  $\alpha' \rightarrow 0$  and planar mixing layers and wakes dominate  $L_z$ . Using these expressions, the zone  $z_c$  (at which  $\bar{w}$  switches signs) can be evaluated by setting  $L_x = L_z$ . Hence, we find that

$$\frac{z_c}{h_c} = \frac{1}{k \alpha'} \left( \lambda d_r - k h_c \left( 1 - \frac{d_o}{h_c} \right) (1 - \alpha') \right).$$

Note that  $\alpha'$  and  $d_o / h_c$  also vary with  $n$ . From previous experiments (Poggi et al. 2004), simplified estimates of these relationships are

$$\alpha' \approx \min \left( 1, \frac{n d_r}{2} \right); \quad \frac{d_o}{h_c} \approx \min \left( 0.85, \frac{0.85}{2} d_r n \right).$$

When  $z > z_c$ ,  $\bar{w}''$  is negative, and conversely, when  $z < z_c$ ,  $\bar{w}''$  is positive.

Figure 8 shows the predicted variation of  $\bar{w}$  as a function of the rod density for two plausible  $\lambda$  ( $=5, 9$ ) along with the measured  $\bar{w}$  inferred from the measured profiles of  $\bar{w}''$  at the hotspot. We comment on a number of features in Fig. 8:

- (1) The scaling analysis proposed here captures the basic patterns of measured  $\bar{w}$  and is suggestive that  $L_x / L_z$  plays an important role in determining the sign of  $\bar{w}$  at the hotspot, with  $L_x$  (and  $L_y$ ) dominated by the size of von Kármán street eddies (proportional to  $d_r$ ) and  $L_z$  by the canonical mixing length for vertical momentum transport. The latter is highly sensitive to the rod density, while the former is not. The lower region dominated by a positive  $\bar{w}$  is, on average, 0.75  $d_r$  thick but this thickness varies with rod density in a nonlinear manner (as shown in

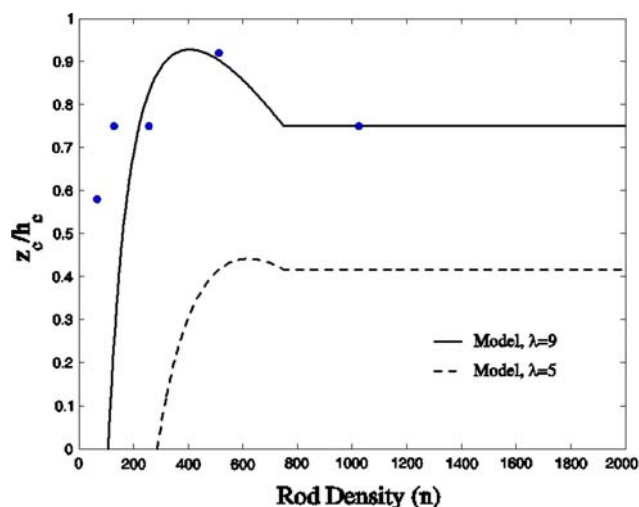


Fig. 8 Variations of the normalized height  $z/h_c$  at which  $\bar{w}''$  switches sign from positive (when  $z < z_c$ ) to negative (when  $z > z_c$ ) as a function of stem density  $n$ . Model calculations are for  $L_x = \lambda d_r$ , where  $d_r$  is the rod diameter, and  $L_x$  is a characteristic longitudinal distance chosen here to represent about one (5) and two ( $\lambda \approx 9$ ) von Kármán street vortex sizes. The data points were determined from the sign shift of the measured profiles in the hotspot behind the rod for all rod densities

Fig. 8). The choice of  $0.7z_c$  in the quadrant analysis shown in Fig. 6 was based on the analysis here.

- (3) The small magnitude of dispersive stresses for dense canopies, when compared to sparse canopies (Fig. 6), can now be predicted from  $\bar{w}'' \sim \bar{u}(L_x/L_z - L_z/L_x)$ . At the hotspot  $\bar{w}''$  (and  $\langle \bar{w}'' \bar{u}'' \rangle$ ) remain small due to the small  $\bar{u}$  (and  $\bar{v}$ ) inside dense canopies, and conversely for sparse canopies.
- (4) Because  $\bar{u}''$  is negative at the hotspot, the strong negative correlation between  $\bar{w}''$  and  $\bar{u}''$  in Fig. 6 is consistent with  $\bar{w}'' \sim \bar{u}(L_x/L_z - L_z/L_x)$ . Extreme values populating quadrant four of Fig. 6 originate from the pressure perturbations described in Sect. 2, while those populating quadrant three originate from the reduced mean continuity effects.

In sum, the scaling analysis here does provide a unifying framework to transition from the mechanisms controlling  $\bar{w}''$  discussed in Sect. 5.2 to those discussed in Sect. 5.1. It can also be employed to explain the outcome of the quadrant analysis in Fig. 6.

### 6 Conclusions

The three dimensional variability in canopy morphology often necessitates a planar averaging operation to the scale of interest. Because of the multiply-connected spaces explored—within the canopy, such spatial averaging gives rise to dispersive terms produced from the spatially

correlations of time-averaged quantities that remain “unclosed” or require further parameterization. To date, parameterizations of these dispersive terms remain illusive, in part because of the limited experiments dedicated to quantifying them. As a first step towards their parameterization, it is necessary to estimate their magnitude, their sign, possible correlations with conventional Reynolds stresses, and any spatial coherency that may be exploited in phenomenological models. Flume experiments for various canopy densities were used to explore these aspects for a cylindrical canopy where the rod density was varied but the single rod attributes were identical. Quadrant analysis was used to explore the spatial coherency of these dispersive stresses at various heights and for a wide range of canopy densities. When compared to the conventional momentum flux, we found that these dispersive stresses in the lowest layers of sparse canopies can be significant (80%). For dense canopies, the dispersive stresses remain negligible when compared to the conventional momentum stresses throughout (<10%).

An analysis on the constitutive components of the dispersive stresses revealed that the positions contributing most to the dispersive terms were localized in the immediate vicinity downstream of the rods (termed here as hotspots). In the deeper canopy layers, their contribution is negative, but in the upper layers, their contribution is positive. The genesis of the sign shift originates from the interplay between the behaviour of the pressure immediately behind the rods and the reduced continuity equation. The fact that  $\bar{w}$  remains positive downstream from the rods over a significant portion of the canopy depth (i.e. bottom 75%) has important implications on a number of applications. For example, long-term measurements of net ecosystem  $\text{CO}_2$  exchange (NEE) are now routinely employed to estimate ecosystem carbon budgets using eddy covariance (EC) methods, yet the large error in the measurement of ecosystem respiration (RE) remains an unresolved problem that must be confronted. The reason this problem is pervasive for  $\text{CO}_2$  transport inside tall canopies is due to the large  $\text{CO}_2$  contribution from the forest floor. EC methods typically measure the turbulent  $\text{CO}_2$  flux above the canopy and neglect any advective (horizontal or vertical) contribution. However, almost all studies, reviewed in Juang et al. (2006) suggest that EC methods do underestimate NEE because of their underestimation of respiratory terms. The “chimney” effect, or the vertical advective flow of  $\text{CO}_2$  immediately adjacent tree stems may provide some clues as to why EC methods underestimate respiration. Whether such “chimney” effect persists in real canopies or not remains to be explored—as branches and foliage may intercept and disperse the rising  $\text{CO}_2$  (except perhaps during leaf-less winter conditions in hardwood forests). At minimum, the

findings here should motivate future smoke release experiments in the field. Likewise, in benthic boundary layers, such “chimney” effects can contribute to rapid transport of nutrients from the soil pore space to the photosynthetic tissues of the aquatic plants (Nepf and Kolar 1999).

More broadly, there are a number of reasons why exploring dispersive fluxes is a timely topic. The rapid progress in canopy LIDARS (light detection and ranging) are now permitting unprecedented view of foliage variation and canopy morphology (Harding et al. 2001; Parker et al. 2001; Lefsky et al. 2002). Hence, the ability to quantify the statistical attributes of the canopy morphology is progressing rapidly. What is clearly lacking is how to link such variability with the spatially-averaged flow dynamics needed in any rigorous upscaling efforts. Dispersive terms provide the theoretical under-pinning of such linkages, and hence, exploring their magnitude and importance should be a logical first step. The advent of experimental techniques such as particle image velocity (PIV) meters, laser induced fluorescence (LIF) measurement techniques, and LDA are now permitting basic experiments to be carried out on these dispersive terms so that linkages between their statistical structure and basic canopy morphologies can be examined with unprecedented resolution. Such experiments do provide the necessary bench-mark data sets to derive and test phenomenological models linking dispersive fluxes to canopy morphology.

**Acknowledgments** This research was supported, in part, by the National Science Foundation (NSF-EAR 06-35787 and NSF-EAR-06-28432), the United States-Israel Binational Agricultural Research and Development (BARD, Research Grant No. IS3861-06), and the US Department of Energy (DOE) through the office of Biological and Environmental Research (BER) Terrestrial Carbon Processes (TCR) program (Grants # 10509-0152, DE-FG02-00ER53015, and DE-FG02-95ER62083).

## References

- Achenbach E (1968) Distribution of local pressure and skin friction around a circular cylinder in cross-flow up to  $Re = 5 \times 10^6$ . *J Fluid Mech* 34:625–639
- Belcher SE (2005) Mixing and transport in urban areas. *Philos Trans R Soc Math Phys Eng Sci* 363(1837):2947–2968
- Bohm M, Finnigan JJ, Raupach MR (2000) Dispersive fluxes and canopy flows: just how important are they? In: American Meteorology Society, 24th conference on agricultural and forest meteorology, August 14–18, 2000, University of California, Davis, pp 106–107
- Cava D, Katul GG, Scrimieri A, Poggi D, Cescatti A and Giostra U (2006) Buoyancy and the sensible heat flux budget within dense canopies. *Bound Layer Meteorol* 118(1):217–240
- Cheng H, Castro IP (2002) Near wall flow over urban-like roughness. *Bound Layer Meteorol* 104(2):229–259
- Christen A, Vogt R (2004) Direct measurement of dispersive fluxes within a cork oak plantation. In: 26th AMS conference on agricultural and forest meteorology, Vancouver
- Coceal O, Thomas TG, Castro IP, Belcher SE (2006) Mean flow and turbulence statistics over groups of urban-like cubical obstacles. *Bound Layer Meteorol* 121(3):491–519
- Finnigan J (2000) Turbulence in plant canopies. *Ann Rev Fluid Mech* 32:519–571
- Harding DJ, Lefsky MA, Parker GG, Blair JB (2001) Laser altimeter canopy height profiles—Methods and validation for closed-canopy, broadleaf forests. *Remote Sens Environ* 76(3):283–297
- Hsieh CI, Katul G, Chi T (2000) An approximate analytical model for footprint estimation of scalar fluxes in thermally stratified atmospheric flows. *Adv Water Resour* 23(7):765–772
- Juang JY, Katul GG, Siqueira MBS, Stoy PC, Palmroth S, McCarthy HR, Kim HS, Oren R (2006) Modeling nighttime ecosystem respiration from measured CO<sub>2</sub> concentration and air temperature profiles using inverse methods. *J Geophys Res Atmos* 111(D8)
- Katul GG, Albertson JD (1998) An investigation of higher-order closure models for a forested canopy. *Bound Layer Meteorol* 89(1):47–74
- Katul GG, Albertson JD (1999) Modeling CO<sub>2</sub> sources, sinks, and fluxes within a forest canopy. *J Geophys Res Atmos* 104(D6):6081–6091
- Katul GG, Chang WH (1999) Principal length scales in second-order closure models for canopy turbulence. *J Appl Meteorol* 38(11):1631–1643
- Katul G, Hsieh CI, Bowling D, Clark K, Shurpali N, Turnipseed A, Albertson J, Tu K, Hollinger D, Evans B, Offerle B, Anderson D, Ellsworth D, Vogel C and Oren R (1999) Spatial variability of turbulent fluxes in the roughness sublayer of an even-aged pine forest. *Bound Layer Meteorol* 93(1):1–28
- Katul GG, Mahrt L, Poggi D, Sanz C (2004) One- and two-equation models for canopy turbulence. *Bound Layer Meteorol* 113(1):81–109
- Katul GG, Porporato A, Nathan R, Siqueira M, Soons MB, Poggi D, Horn HS, Levin SA (2005) Mechanistic analytical models for long-distance seed dispersal by wind. *Am Nat* 166(3):368–381
- Lefsky MA, Cohen WB, Parker GG, Harding DJ (2002) Lidar remote sensing for ecosystem studies. *Bioscience* 52(1):19–30
- Macdonald RW (2000) Modelling the mean velocity profile in the urban canopy layer. *Bound Layer Meteorol* 97(1):25–45
- Macdonald RW, Coulson BJ, Slawson PR (2000) Near field dispersion in the urban environment—a hydraulic time study. *Environ Monitor Assess* 65(1–2):231–238
- Martilli A, Santiago JL (2007) CFD simulation of air flow over a regular array of cubes. Part II: analysis of spatial average properties. *Bound Layer Meteorol* 122(3):635–654
- Nathan R, Katul GG (2005) Foliage shedding in deciduous forests lifts up long-distance seed dispersal by wind. *Proc Natl Acad Sci USA* 102(23):8251–8256
- Nathan R, Katul GG, Horn HS, Thomas SM, Oren R, Avissar R, Pacala SW, Levin SA (2002) Mechanisms of long-distance dispersal of seeds by wind. *Nature* 418(6896):409–413
- Nepf HM, Koch EW (1999) Vertical secondary flows in submersed plant-like arrays. *Limnol Oceanogr* 44(4):1072–1080
- Nikora V, Goring D, McEwan I, Grifths G (2001) Spatially averaged open-channel flow over rough bed. *J Hydraul Eng ASCE* 127(2):123–133
- Parker GG, Lefsky MA, Harding DJ (2001) Light transmittance in forest canopies determined using airborne laser altimetry and in-canopy quantum measurements. *Remote Sens Environ* 76(3):298–309
- Poggi D, Katul GG (2006) Two-dimensional scalar spectra in the deeper layers of a dense and uniform model canopy. *Bound Layer Meteorol* 121(2):267–281

- Poggi D, Katul GG (2007) Turbulent flows on forested hilly terrain: the recirculation region. *Q J R Meteorol Soc* 133(625):1027–1039
- Poggi D, Porporato A, Ridol L (2003) Analysis of the small-scale structure of turbulence on smooth and rough walls. *Phys Fluids* 15(1):35–46
- Poggi D, Katul GG, Albertson JD (2004a) Momentum transfer and turbulent kinetic energy budgets within a dense model canopy. *Bound Layer Meteorol* 111(3):589–614
- Poggi D, Katul GG, Albertson JD (2004b) A note on the contribution of dispersive fluxes to momentum transfer within canopies—research note. *Bound Layer Meteorol* 111(3):615–621
- Poggi D, Porporato A, Ridol L, Albertson JD, Katul GG (2004c) The effect of vegetation density on canopy sub-layer turbulence. *Bound Layer Meteorol* 111(3):565–587
- Poggi D, Katul GG, Albertson JD, Ridol L (2007) An experimental investigation of turbulent flows over a hilly surface. *Phys Fluids* 19(3)
- Pokrajac D, Campbell LJ, Nikora V, Manes C, McEwan I (2007) Quadrant analysis of persistent spatial velocity perturbations over square-bar roughness. *Exp Fluids* 42(3):413–423
- Raupach MR, Shaw RH (1982) Averaging procedures for flow within vegetation canopies. *Bound Layer Meteorol* 22(1):79–90
- Raupach MR, Coppin PA, Legg BJ (1986) Experiments on scalar dispersion within a model-plant canopy. 1. The turbulence structure. *Bound Layer Meteorol* 35(1–2):21–52
- Ruck B, Adams E (1991) Fluid mechanical aspects of the pollutant transport to coniferous trees. *Bound Layer Meteorol* 56(1–2):163–195
- Siqueira M, Lai CT, Katul G (2000) Estimating scalar sources, sinks, and fluxes in a forest canopy using Lagrangian, Eulerian, and hybrid inverse models. *J Geophys Res Atmos* 105(D24):29475–29488
- Soons MB, Heil GW, Nathan R, Katul GG (2004) Determinants of long-distance seed dispersal by wind in grasslands. *Ecology* 85(11):3056–3068